Pattern Recognition 127 (2022) 108607

Contents lists available at ScienceDirect

Pattern Recognition

journal homepage: www.elsevier.com/locate/patcog

Non-separable rotation moment invariants

Leonid Bedratyuk[a], Jan Flusser[b,*], Tomáš Suk[b], Jitka Kostková[b], Jaroslav Kautsky[c]

[a] Khmelnytsky National University, Instytuts'ka, 11, Khmelnytsky 29016, Ukraine
[b] Czech Academy of Sciences, Institute of Information Theory and Automation, Pod Vodárenskou věží 4, Prague 8 182 08, Czech Republic
[c] The Flinders University of South Australia, GPO Box 2100, Adelaide, SA 5001, Australia

ARTICLE INFO

Article history:
Received 10 January 2021
Revised 16 February 2022
Accepted 21 February 2022
Available online 22 February 2022

Keywords:
Image recognition
Rotation invariants
Non-separable moments
Appell polynomials
Bi-orthogonality
Recurrent relation

ABSTRACT

In this paper, we introduce new rotation moment invariants, which are composed of non-separable Appell moments. We prove that Appell polynomials behave under rotation as monomials, which enables easy construction of the invariants. We show by extensive tests that non-separable moments may outperform the separable ones in terms of recognition power and robustness thanks to a better distribution of their zero curves over the image space.

1. Introduction

Moments and moment invariants have established a popular and widely-used category of "handcrafted" features for object description and recognition (see Flusser et al. [1] for a comprehensive survey). From the mathematical point of view, the moments are projections of the image function onto a basis formed by polynomials. Although all polynomial bases of the same degree are theoretically equivalent in the sense that they all generate the same subspace, hundreds of experiments performed in the last 60 years have shown that their performance in object recognition experiments is different. The differences are caused mostly by the way how individual polynomials are evaluated, by numerical stability of these algorithms, by test objects, and also by the overall setup of the experiment. Although the results of some papers are not very convincing or even contradict other reported results, one can trace a few trends and conclusions that the majority of the authors have agreed on.

A "globally optimal" polynomial basis that would always outperform the others apparently does not exist. Among other reasons, this is because the recognition power depends not only on the chosen features (moments) but also on the data themselves. Most authors tend towards using orthogonal polynomials (OP) because they provide on average a better recognition rate than non-orthogonal ones thanks to efficient and stable recurrent algorithms for their computation and low correlation between individual polynomials. When dealing with 2D images, all authors have used *separable* 2D polynomials that are a straightforward but rather limiting extension of 1D ones.

However, separable polynomials have certain intrinsic limitations in their recognition power, as is analyzed later in the paper.

The reason why *non-separable* polynomials and moments have not been tested for pattern recognition purposes is probably twofold. First, no moment invariants to image rotation constructed from non-separable moments have been published yet. Since rotation invariance (along with translation and scale invariance) is required in almost all practical situations, this has been in our opinion the main obstacle. Second, only a few non-separable polynomials can be efficiently calculated in a fast and stable way.

To expose our hypothesis why non-separable moments could outperform the separable ones, let us recall the main factors that determine the ability of polynomials to represent an image function. The number of zeros should be as high as possible and the zeros should be evenly distributed over the image plane (the zeros should not be concentrated in any subarea of the image and the region size between the zeros should be small and constant). The range of values of the polynomial between any two zeros should be approximately the same, which leads to locally constant representation ability no image subarea is preferred/suppressed). Already in the 1980s, Mostafa and Psaltis [2] studied these properties of separable complex monomials and showed how they affect the

* Corresponding author.
E-mail addresses: leonid.uk@gmail.com (L. Bedratyuk), flusser@utia.cas.cz (J. Flusser), suk@utia.cas.cz (T. Suk), kostkova@utia.cas.cz (J. Kostková), Jerry.Kautsky@flinders.edu.au (J. Kautsky).

https://doi.org/10.1016/j.patcog.2022.108607
0031-3203/

representation ability. However, nobody has tested them for non-separable polynomials. Yet another aspect that may influence the recognition ability is the following. Zero curves of separable polynomials always have to follow the raster, either Cartesian or polar. Hence, they represent better the image structures in the raster directions than in the "diagonal" directions. Our hypothesis is that properly chosen non-separable polynomials may exhibit zero-curve patterns, which are in the above-mentioned sense better for image representation than those of any separable polynomials.

In this paper, we introduce for the first time rotation invariants composed of non-separable bi-orthogonal moments. That is the main theoretical result of the paper. To reduce the computing complexity and maintain numerical stability, we present recursive formulae for their efficient evaluation. We show by extensive tests on noise-free and noisy images that non-separable moments may outperform the separable ones in recognition power and robustness.

2. Separable and non-separable polynomials

Bivariate polynomial $\pi_{pq}(x,y)$ of degree $p+q$ is called *separable* if it can be factorized as $\pi_{pq}(x,y)=\beta_p(x)\gamma_q(y)$, where $\beta_p(x)$ and $\gamma_q(y)$ are univariate polynomials of degree p and q, respectively. Any polynomial $\pi_{pq}(x,y)$, regardless of its (non-)separability, generates moment $M_{pq}(x,y)$ of image $f(x,y)$

$$M_{pq}=\int_{-\infty}^{\infty}\int_{-\infty}^{\infty}\pi_{pq}(x,y)f(x,y)\,\mathrm{d}x\,\mathrm{d}y \tag{1}$$

(provided that the integral converges) that can be understood as a projection of $f(x,y)$ onto $\pi_{pq}(x,y)$.

All 2D polynomials, that have been used in pattern recognition to generate moments as object features, are separable. The separability is either in the Cartesian domain, such as pure monomials [3], Legendre moments [4–6], Chebyshev moments [7–9], Hermite and Gaussian–Hermite moments [10–13], Krawtchouk moments [14], and Gegenbauer moments [15], or in polar coordinates as in the cases of Zernike moments [16–18], pseudo-Zernike moments [19], Fourier–Mellin moments [20,21], Jacobi–Fourier moments [22], and Chebyshev–Fourier moments [23].

On the one hand, separable polynomials are attractive to work with because they are easy to express and calculate (many sophisticated computing algorithms have been published recently, see for instance [24–26]). On the other hand, a common drawback is their constrained distribution of zeros. The zeros always fill a (generally irregular) rectangular grid. When these polynomials are used as basis functions, they provide better resolution in the grid direction, which means in the direction of the coordinates. The resolution in close-to-diagonal directions is worse. Although this effect is not significant if a sufficiently high degree is used, it still may lead to the drop of discriminability if characteristic object structures exhibit a diagonal-like orientation. Recently, some authors have tried to compensate for this effect by using polar harmonic or exponential basis functions instead of polynomials [27] and by introducing fractional-order moments [28–30] but all these have led to a slight improvement only since the limitation imposed by the separability of the basis has not been removed. Non-separable polynomials, a distribution of zeros of which may be almost arbitrary, do not suffer from this drawback.

3. Quasi-monomials and rotation invariants

Rotation $(x,y)\mapsto(x',y')$ by angle θ is given as

$$\begin{aligned}x'&=x\cos\theta-y\sin\theta,\\ y'&=x\sin\theta+y\cos\theta.\end{aligned} \tag{2}$$

The monomials $x^m y^n$ are transformed under rotation as

$$(x')^m(y')^n=\sum_{i=0}^{m}\sum_{j=0}^{n}(-1)^i\binom{m}{i}\binom{n}{j}(\cos\theta)^{m-i+j}(\sin\theta)^{n-j+i}x^{m+n-i-j}y^{i+j}. \tag{3}$$

Grouping the variables of the same power together, Eq. (3) can be rewritten into the form

$$(x')^m(y')^n=\sum_{r=0}^{m+n}k(r,m,n,\theta)x^{m+n-r}y^r\,, \tag{4}$$

where $k(r,m,n,\theta)$ is a coefficient given as a linear combination of certain powers of $\sin\theta$ and $\cos\theta$ (see Yang et al. [12] for explicit forms of $k(r,m,n,\theta)$).

Flusser [31] proposed a general theory that allows constructing a complete and independent set of rotation invariants of arbitrary order (see also Bedratyuk [32] for a group-theoretical viewpoint of the same problem). It was originally developed for monomials and corresponding geometric moments but it can be applied to any polynomials and their moments which are transformed under rotation in the same way as the monomials. Such polynomials are called *quasi-monomials* and play an important role in the theory and practice of rotation invariants.

Definition. Polynomial family $\{B_{m,n}(x,y)\}$ is called quasi-monomial (QM) family if it is transformed under rotation (2) as

$$B_{m,n}(x',y')=\sum_{r=0}^{m+n}k(r,m,n,\theta)B_{m+n-r,r}(x,y)\,, \tag{5}$$

where the coefficients $k(r,m,n,\theta)$ are the same as those in (4).

This idea was used by Yang et al., who proved that Hermite polynomials are quasi-monomials [12,13] and derived formulas for Hermite rotation invariants of arbitrary orders [33]. Later on, the same authors proved that Hermite polynomials (up to scaling and modulation) are the only existing quasi-monomials among all separable orthogonal polynomials [34].

In the next section, we prove the existence of non-separable quasi-monomials, which allows us to adopt the theory from Flusser [31] and to use these polynomials as a basis for designing rotation invariants.

4. Appell bi-orthogonal polynomials

First, we formulate a necessary and sufficient condition for a polynomial to be a quasi-monomial. Then we introduce *Appell polynomials*, prove they are quasi-monomials, and present recursive relations for their computation.

The following theorem presents a simple criterion for the quasi-monomiality of a polynomial family in terms of its generating function.

Theorem 1. *The polynomial family* $\{B_{m,n}(x,y)\}$ *defined by generating function*

$$G(x,y,u,v)=\sum_{m,n=0}^{\infty}B_{m,n}(x,y)\frac{u^m}{m!}\frac{v^n}{n!}$$

is a quasi-monomial if and only if G *is a function of* $ux+vy, x^2+y^2$ *and* u^2+v^2 *only.*

See Appendix A for the proof.

The QM property might be lost if the polynomials have been scaled by multiplicative constants, which is often applied to keep the range of values reasonably bounded. The following theorem explores what kind of scaling preserves the QM property.

Theorem 2. *Let $\{B_{m,n}(x,y)\}$ be a quasi-monomial family. The polynomial family $\{\widetilde{B}_{m,n}(x,y)\}$, where*

$$\widetilde{B}_{m,n}(x,y) = \alpha_{m,n} B_{m,n}(x,y)\,,$$

is a quasi-monomial if and only if each coefficient $\alpha_{m,n}$ is a function of $m+n$ only.

See Appendix B for the proof.

Let us consider two polynomial families $\{V_{m,n}(x,y)\}$ and $\{U_{m,n}(x,y)\}$ defined by generating functions

$$\frac{1}{1-2(ux+vy)+u^2+v^2} = \sum_{m,n=0}^{\infty} V_{m,n}(x,y)\frac{u^m}{m!}\frac{v^n}{n!}\,,$$

$$\frac{1}{\left[(1-(ux+vy))^2-\left(u^2+v^2\right)\left(x^2+y^2-1\right)\right]^{\frac{1}{2}}} = \sum_{m,n=0}^{\infty} U_{m,n}(x,y)\frac{u^m}{m!}\frac{v^n}{n!}.$$

These polynomials are known as *Appell polynomials* (AP).[1] They are non-separable both in Cartesian as well as polar domains. As follows directly from Theorem 1, AP's are quasi-monomials.

Appell polynomials can be expressed explicitly as

$$V_{m,n}(x,y) = m!n!\,2^{m+n}\sum_{i=0}^{\lfloor\frac{m}{2}\rfloor}\sum_{j=0}^{\lfloor\frac{n}{2}\rfloor}(-1)^{i+j}\frac{(m+n-i-j)!}{i!\,j!\,(m-2i)!\,(n-2j)!\,2^{2(i+j)}}x^{m-2i}y^{n-2j},$$

$$U_{m,n}(x,y) = \frac{m!n!}{2^{m+n}}\sum_{k=0}^{m+\lfloor\frac{n}{2}\rfloor}\sum_{j=\lceil\frac{m}{2}\rceil}^{k}(-1)^{j-k}\binom{m+n}{k}\binom{k}{j}\binom{2j}{m}\binom{2m+2n-2k}{n}\cdot x^{2j-m}y^{2(m-k)+n},$$

where the brackets $\lfloor a\rfloor$ and $\lceil a\rceil$ stand for integer "floor" and "ceiling" of a, respectively.

Appell polynomials U and V form a bi-orthogonal system on the unit disc $B=\{(x,y)|x^2+y^2\le 1\}$, where the relation of bi-orthogonality is

$$\iint_B V_{m,n}(x,y)U_{p,q}(x,y)\,\mathrm{d}x\,\mathrm{d}y = \frac{\pi\,(m+n)!\,m!\,n!}{m+n+1}\,\delta_{mp}\,\delta_{nq} \tag{6}$$

(see Didon [35] for the proof).

When calculating the Appell polynomials numerically using the explicit formulae, we may face precision loss due to floating-point overflow and/or underflow. This phenomenon is well known from many 1D orthogonal polynomials, where it is overcome thanks to three-term recurrent relations (we refer to Favard's Theorem [36]). Although Favard's Theorem generally does not hold for 2D bi-orthogonal polynomials, in the case of Appell polynomials the following recurrences can be used for their efficient and stable computation.

Theorem 3. *Polynomials $V_{m,n}(x,y)$ satisfy the four-term recurrence relations*

$$\begin{aligned}2(1+m+n)xV_{m,n}(x,y) =& V_{m+1,n}(x,y) - n(n-1)V_{m+1,n-2}(x,y)\\ &+ m(m+2n+1)V_{m-1,n}(x,y)\,,\end{aligned} \tag{7}$$

$$\begin{aligned}2(1+m+n)yV_{m,n}(x,y) =& V_{m,n+1}(x,y) - m(m-1)V_{m-2,n+1}(x,y)\\ &+ n(n+2m+1)V_{m,n-1}(x,y)\,,\end{aligned} \tag{8}$$

with the initial condition $V_{0,0}(x,y)=1$ and adopting the convention that if m or n is/are negative, then $V_{m,n}$ is considered zero.

See Appendix C for the proof.

Theorem 4. *Polynomials $U_{m,n}(x,y)$ satisfy the five-term recurrence relations*

$$\begin{aligned}U_{m+1,n}(x,y) =& (n+2m+1)xU_{m,n}(x,y) + mnxyU_{m,n-1}(x,y)\\ &- mn(m+n-1)yU_{m-1,n-1}(x,y)\\ &+ m\left[\left(y^2-1\right)m + n\left(2y^2-1\right)\right]U_{m-1,n}(x,y)\,,\end{aligned} \tag{9}$$

$$\begin{aligned}U_{m,n+1}(x,y) =& (m+2n+1)yU_{m,n}(x,y) + mnxyU_{m-1,n}(x,y)\\ &- mn(m+n-1)xU_{m-1,n-1}(x,y)\\ &+ n\left[\left(x^2-1\right)n + m\left(2x^2-1\right)\right]U_{m,n-1}(x,y)\,,\end{aligned} \tag{10}$$

with the initial condition $U_{0,0}(x,y)=1$ and adopting the convention that if m or n is/are negative, then $U_{m,n}$ is considered zero.

See Appendix D for the proof.

The graphs of Appell polynomials U and V up to the degree 10 are shown in Figs. 1 and 2. One may observe two important properties. Individual polynomials have distinct "preferred directions" controlled by the indices m and n. This differentiates the AP's from separable polynomials that always prefer the raster direction. When comparing U and V, we can see that the V-polynomials exhibit high values and big fluctuations near the boundary of the unit disc and are relatively flat inside it, so there is a big information suppression in the central area and a preference of the boundary area. On the contrary, the U-polynomials do not exhibit such big differences and do not systematically emphasize any subarea. This is why we expect U to be more discriminative and also more robust to noise than V.

Finally, we investigated the zero-curve patterns of U and V and compared them with two well-established kinds of separable polynomials – Gaussian–Hermite (GH) [13] and Zernike (Z) [16]. In each case, we calculated the first 30 polynomials and plotted their zero curves, see Fig. 3. It is apparent that the zero curves of separable GH and Z polynomials always follow the raster (GH in the Cartesian domain and Z in the polar domain). Zero curves of U and V may take arbitrary directions, which creates a kind of "random" patterns. The zeros of U and V partition the image domain more uniformly. To evaluate the distribution quantitatively, we calculated the size of each area and computed the mean and standard deviation. The results in the form of (mean; std) are the following: $U\sim(0.01;\ 0.05)$, $V\sim(0.02;\ 0.06)$, $Z\sim(0.27;\ 0.64)$, and GH $\sim(0.33;\ 0.96)$ (the numbers are in % of the unit circle in case of U,V and Z and in % of the unit square in case of the GH polynomials). Both the mean and the standard deviation are minimal for the U polynomials (and more than ten times lower than those of GH and Z), which clearly supports our hypothesis formulated in the introduction.

5. Appell rotation invariants

Thanks to the fact that the AP's are quasi-monomials, we are ready to adapt the theory of rotation invariants [31] and construct invariants from the Appell moments. This is very easy and elegant – we just take the formula for invariants from geometric moments (i.e. for moments of monomials x^py^q) and replace the geometric moments with the corresponding Appell moments A_{pq} (either with respect to polynomials U or V, both versions work). Doing so, we design the *Appell rotation invariants*

$$\Phi_{pq} = \left(\sum_{k=0}^{q_0}\sum_{j=0}^{p_0}\binom{q_0}{k}\binom{p_0}{j}(-1)^{p_0-j}i^{p_0+q_0-k-j}A_{k+j,\,p_0+q_0-k-j}\right)^{p-q}$$

[1] Named after P.E. Appell, a French mathematician (1855–1930). The name "Appell polynomials" has been commonly used for similar and more general polynomial families. The ones we use in this paper are sometimes referred to also as Didon or Didon–Hermite polynomials.

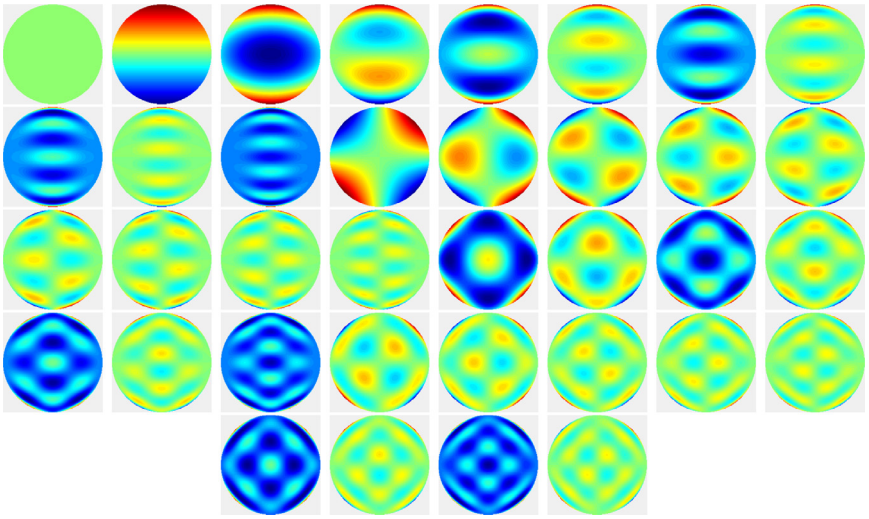

Fig. 1. Appell polynomials U up to the 10th degree.

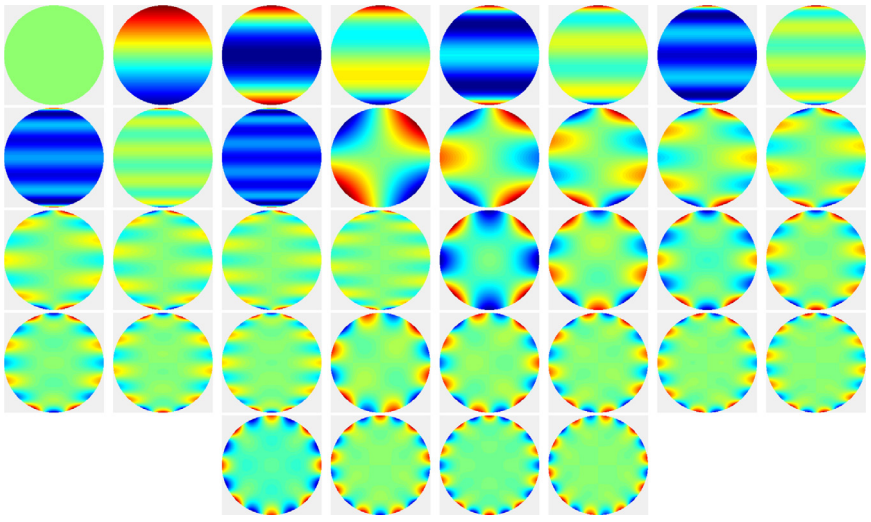

Fig. 2. Appell polynomials V up to the 10th degree.

$$\cdot \sum_{k=0}^{p}\sum_{j=0}^{q}\binom{p}{k}\binom{q}{j}(-1)^{q-j}i^{p+q-k-j}A_{k+j,p+q-k-j} \tag{11}$$

where $p \geq q$ and p_0, q_0 are fixed user-defined indices (preferably very low ones) such that $p_0 - q_0 = 1$ (see Flusser [31] for a detailed derivation of this formula for geometric moments and [1] for a deeper insight and the links to other approaches). As follows from Flusser [31], the set of invariants $\{\Phi_{pq}\}$ is independent and complete because the Appell polynomials form a basis of the image space.

Appell invariants (11) are automatically invariant also to translation and scaling. Unlike most of the other moments, where a special normalization must be introduced, this is achieved as a by-product of the algorithm how the Appell moments are calculated. Since the area of bi-orthogonality is the unit disc B, we map the image onto B such that its centroid coincides with $(0, 0)$ and B circumscribes the image. This mapping is scale and shift-invariant.

To keep the dynamic range of the AP's in a reasonable interval, it is desirable to normalize their values. However, such a normalization must preserve the QM property of the polynomials (see Theorem 2). We recommend using the following normalization, which has been found heuristically and evaluated as the best one

$$\widetilde{V}_{m,n}(x,y) = \frac{m+n+1}{\sqrt{\pi[(m+n)!]^{3/2}\Gamma\left(\frac{m+n}{2}+1\right)}}V_{m,n}(x,y)\,, \tag{12}$$

$$\widetilde{U}_{m,n}(x,y) = \frac{1}{\sqrt{\pi[(m+n)!]^{3/2}\Gamma\left(\frac{m+n}{2}+1\right)}}U_{m,n}(x,y). \tag{13}$$

The recurrent relations must be modified accordingly, see Appendix E.

6. Experiments

We have carried out two kinds of experiments, both aimed at testing the recognition power of the Appell invariants in comparison with traditional separable invariants from Gaussian–Hermite moments [33], Zernike moments [17], and Chebyshev–Fourier (Ch-F) moments [37]. All computations were implemented using efficient recurrent formulae to make the comparison fair. Particularly, Appell moments were calculated using the recurrences given in Appendix E, GH moments by the method from [33], Z moments by Kintner's algorithm [38], and Ch-F moments by the method taken from Li et al. [39].

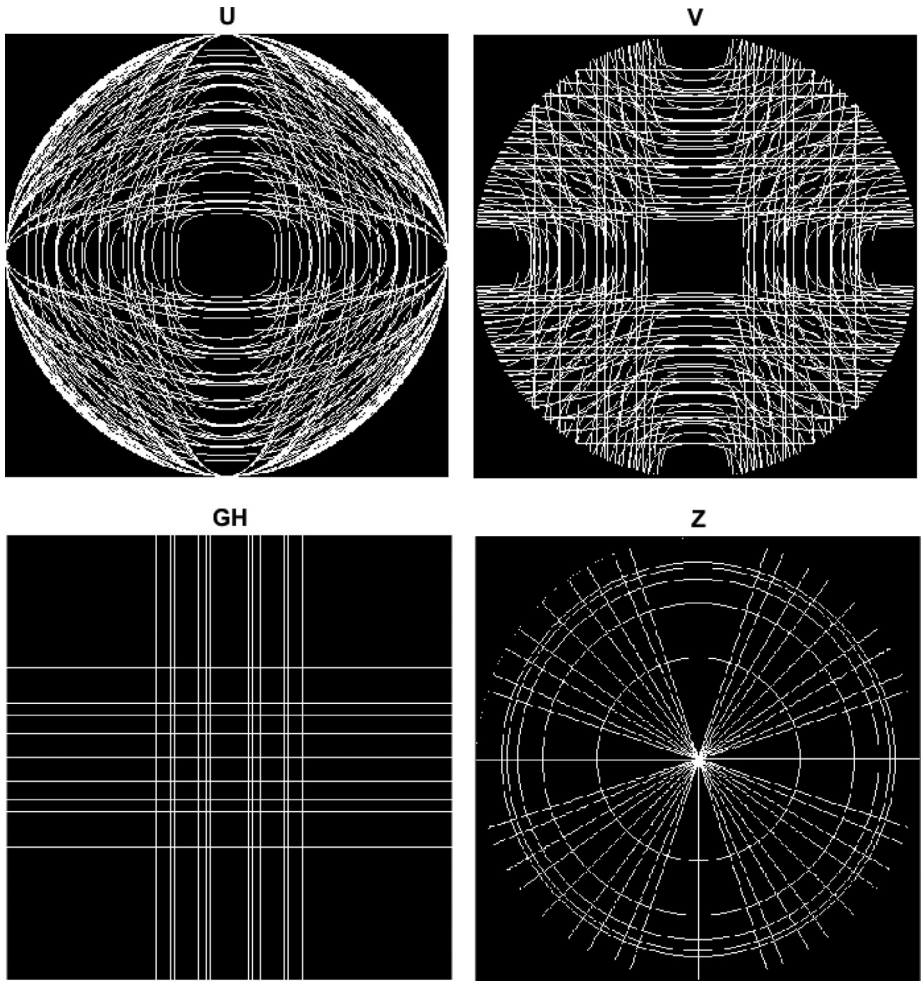

Fig. 3. Zero curves of Appell polynomials U (top left), V (top right), Gaussian–Hermite polynomials (bottom left), and Zernike polynomials (bottom right).

The first experiment is performed on a benchmark dataset of 3D objects rotated artificially to keep the rotation model exactly valid and generate enough samples to get statistically significant results. The second experiment uses real photographs of an indoor scene, where the image rotation is introduced by the rotation of the camera. All codes used in this section are publicly available in a user-friendly form via Gitlab at https://gitlab.com/kostkjit/moment-invariants.

6.1. Recognition of ALOI images

This experiment was performed on publicly available Amsterdam Library of Object Images (ALOI) [40]. We downloaded 1000 images of distinct objects (90 samples are shown in Fig. 4) and rotated each of them 35 times with the step 10°. We used the nearest neighbor interpolation to resample the images (see Fig. 5 for the rotated versions of the test object No. 155). The objects are masked, so the background is zero and does not influence the moment values.

To calculate the invariants of Zernike, Chebyshev–Fourier, Appell V and Appell U moments, the image was mapped onto the unit circle. For Gaussian–Hermite moments, we used the modulation parameter $\sigma = 0.3$ (see Yang et al. [33] for details). In all cases, invariants up to the fourth and fifth orders were applied.

To eliminate random errors and to get a higher significance, we applied a multiple cross-validation. In the first run, we used the original images as the templates and classified all rotated versions. In the second run, the images rotated by 10° were used as the templates, and all others were classified. The classification was performed by a simple minimum-distance rule in the space of the invariants. We repeated this process for all rotations up to 80° (incorporating rotations beyond the first quadrant does not make sense because the results were identical). In this way, the final success rate of each invariant type was calculated from $35 \times 1000 \times 9 = 315,000$ trials.

The results are summarized in Fig. 6. As one can expect, the overall success rate of all invariants is relatively high (the worst error rate is about 0.2%) because the only source of misclassifications is numerical errors of the polynomials and sensitivity to image resampling. Nevertheless, we can identify certain differences in performance. Appell U invariants work without any error, they outperform all the others. Appell V's are the second-best to the fourth order. When increasing the order to five, Gaussian–Hermite invariants become the second-best ones.

The differences between individual polynomial families become more apparent when we are supposed to classify noisy images. To illustrate that, we repeated the entire experiment but this time we corrupted each image with an additive white Gaussian noise of SNR = 15 dB. As can be seen from Fig. 7, the Appell U moments are again the best performing ones. Noise robustness is a property that is difficult to analyze rigorously, but generally, it depends on the shape of the polynomials. Smooth polynomials should be more robust than those with high fluctuations, which corresponds to the shape of Appell U polynomials (see Fig. 1). The superior robustness

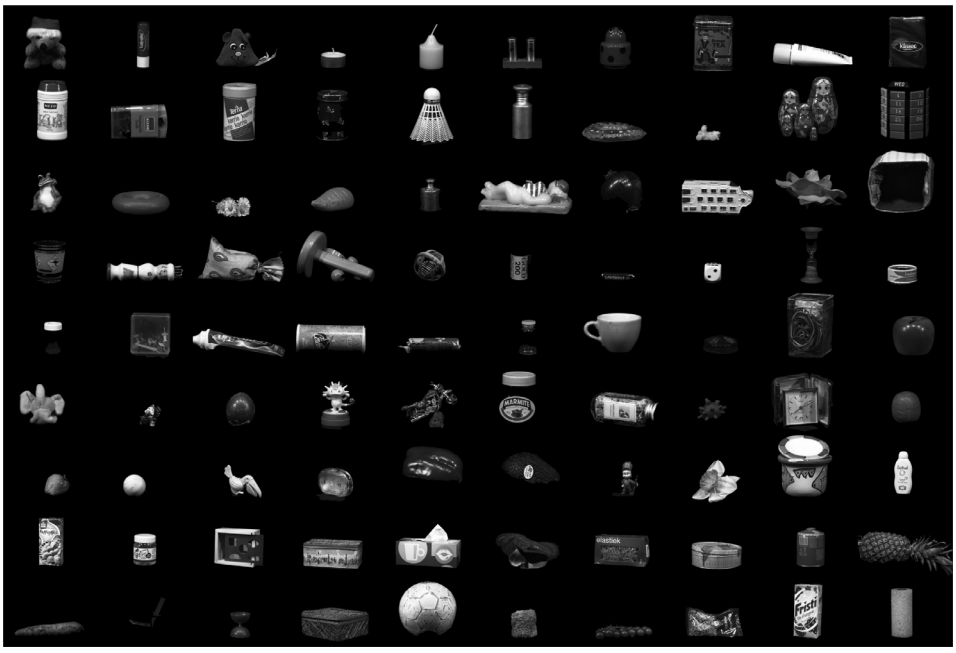

Fig. 4. Sample images of the ALOI dataset used in our experiment.

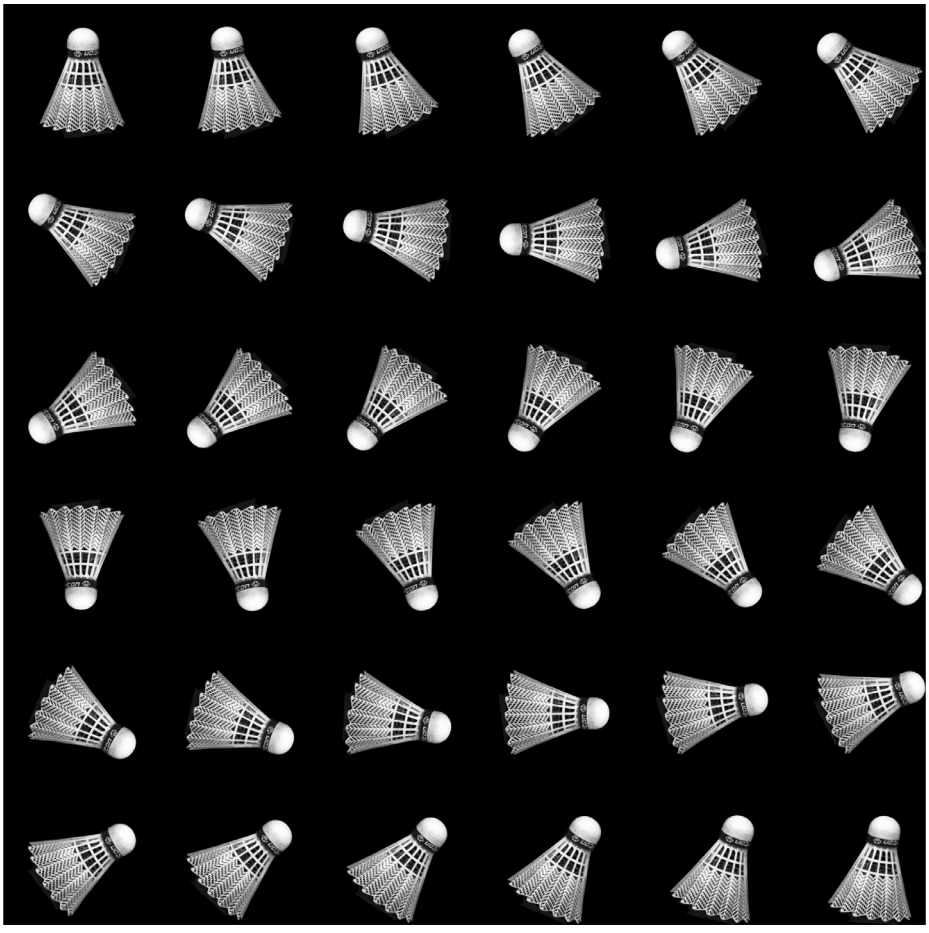

Fig. 5. 36 rotated instances of the test object No. 155 (badminton shuttlecock).

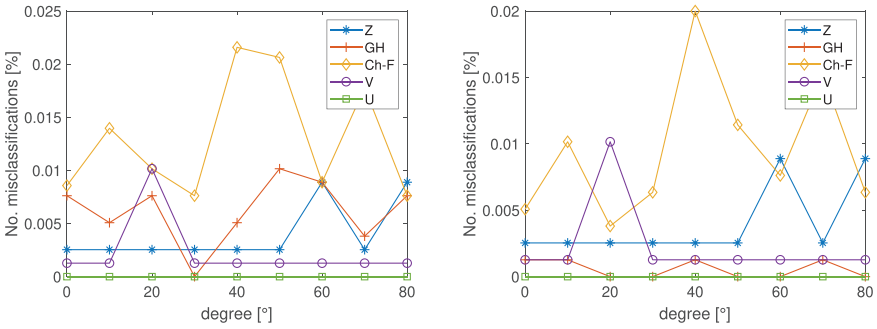

Fig. 6. ALOI experiment: The error rate in % achieved in $9 \times 35\ 000$ trials. Rotation invariants up to the 4th order (left) and 5th order (right) were used. Zernike (Z), Gaussian–Hermite (GH), Chebyshev–Fourier (Ch-F), Appell V (V) and Appell U (U) moments were applied, respectively.

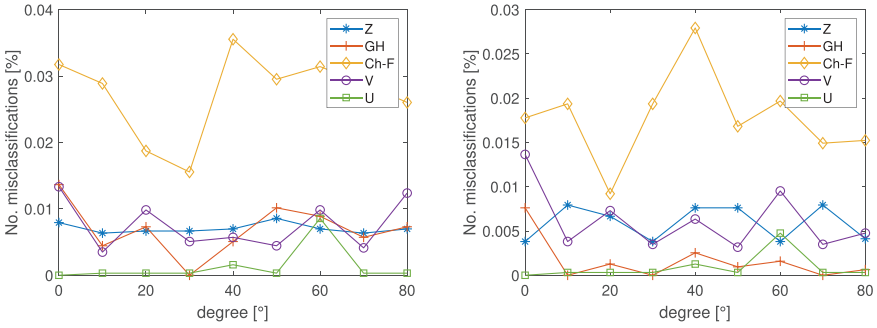

Fig. 7. The same ALOI experiment as in Fig. 6 but all images were corrupted by noise of SNR = 15 dB.

of the Appell U appeared consistently over several runs and various noise instances.

To provide the readers with deeper insight, we measured the noise robustness also in a different way. For 35,000 noisy images, we evaluated the mean relative error (MRE) of Zernike and Appell U moments, which characterizes the moment vulnerability. While MRE of Zernike moments was about 1.6%, MRE of Appell U moments was approximately 0.7%. We tested the same on two other noise levels (SNR = 10 dB and SNR = 20 dB) and discovered that the MRE of Zernike moments is always more than double the MRE of the Appell U.

We can conclude this series of experiments as follows. The Appell U invariants have exhibited the best performance among all moments tested, both on noise-free and noisy data. The superior performance in the noisy case has been achieved thanks to the high robustness of the Appell moments and also due to the fact, that Appell U invariants separate the classes in a noise-free case better than the others. Hence, if the moment values are corrupted because of the noise, the impact on the recognition results is smaller than in the case of the other moments.

6.2. Template matching

Unlike the previous experiment, this one was performed on real photographs of an indoor scene and physical camera rotations along its optical axis to test the behavior of the invariants under real-life conditions. We tried to avoid any other image distortion such as perspective projection, scaling and camera shake blur.[2]

We captured a sequence of nine images of a bookcase with a camera rotation ranging approximately from -90° to $+90^\circ$. We converted RGB to IHS and worked with the intensity only. The frame with "natural" camera orientation served as a reference. In the reference frame, we randomly selected 61 non-overlapping templates with a radius 127 pixels, see Fig. 8, and extracted the same set in all frames. Then we matched the templates from the rotated frames with the reference templates. We also adopted the scenario with cross-validation. We run the experiment nine times such that each of our nine images served just once as the reference frame. Likewise the previous experiment, we compared the matching performance of five moment sets - Zernike, Gaussian–Hermite, Chebyshev–Fourier, Appell V, and Appell U, respectively. We repeated the entire experiment four times, changing the maximum moment order from 7 to 10.

The results are summarized in Fig. 9, where the number of mismatched templates (in %) is shown for each case. Note that in each setting (i.e. for a single method and the given moment order) we matched $61 \times 8 \times 9 = 4392$ templates. We can see the best results were achieved by the Gaussian–Hermite and Appell U moments (both are comparable, yielding about 1% error rate). The other three moment sets performed worse. This is consistent with the previous experiment on ALOI images.

In the case of real photographs, the main source of errors is JPEG compression artifacts, which obviously depend on the camera-to-scene orientation. This is also the reason why the error rate is here almost independent of the maximum moment order (i.e., on the number of the invariants used). Higher-order moments, which theoretically should improve the matching rate since they capture fine details of the templates, are more sensitive to model violations (i.e. to JPEG artifacts and noise) and actually do not contribute to the performance of the invariants.

6.3. Computing complexity

In this section, we investigate the computing complexity of the Appell moments. There is a common concern that non-separable polynomials are computationally expensive. We show that this is not generally true and that the Appell moments can be computed efficiently.

[2] From the mathematical point of view, the invariants are normalized to scaling thanks to the mapping, but in practice, if scaling is unknown, we do not know what is the correct template size.

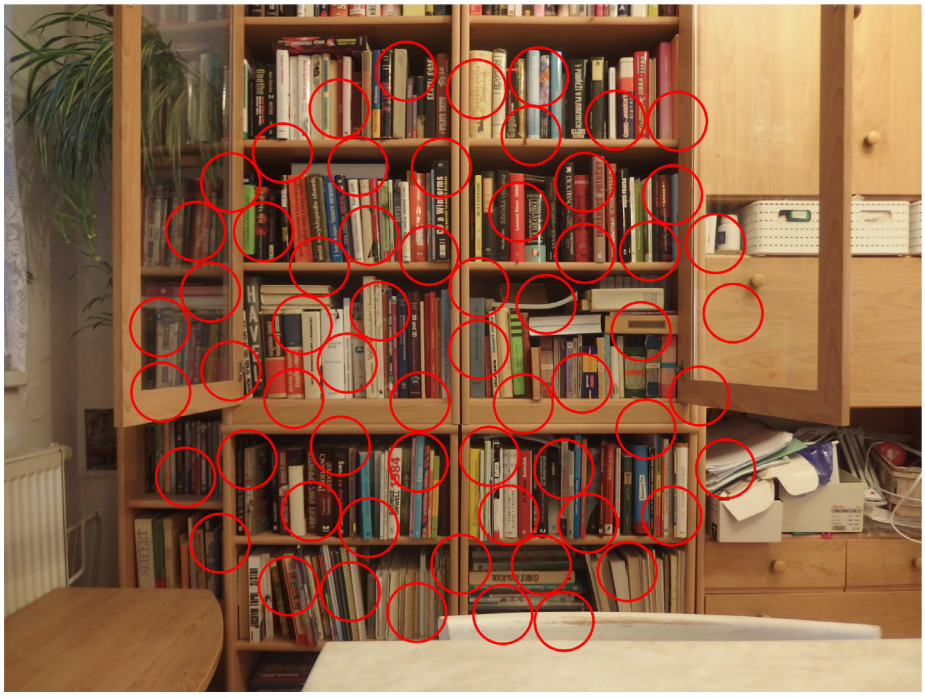

Fig. 8. The reference frame of the sequence with the selected templates. The image size is 3968×2976, the template radius is 127 pixels.

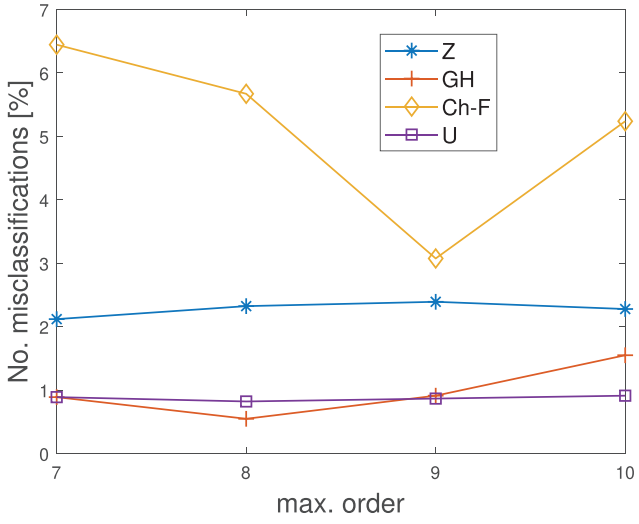

Fig. 9. The error rate (in % of 4392 trials) of various methods for maximum moment orders from 7 to 10. The errors of Appell V range from 16% to 26% and do not fit into the graph.

Theoretical complexity is not very informative. If we compute sampled polynomials on $m \times n$ array, we need $\mathcal{O}(mn(p+q))$ operations for separable polynomials and $\mathcal{O}(mnpq)$ operations for non-separable polynomials. As soon as the polynomials have been pre-calculated, the complexity of a single moment is always $\mathcal{O}(mn)$ regardless of the (non)separability. So, seemingly pq grows much faster than $p+q$, but the constants control the actual speed.

Since the experiments presented in the previous sections use only low-order moments, the differences in the runtimes are insignificant and cannot be measured reliably. So, we performed another experiment devoted solely to the time measurement. We took Lena image 256×256 and calculated all its moments up to the order 100. The total runtime for individual moment types is 2.99 s for Appell U, 2.89 s for Appell V, 8.29 s for Zernike, 8.87 s for Chebyshev-Fourier, and 0.10 s for Gaussian–Hermite moments, respectively. The times include all pre-calculations of the polynomials. The experiment was run in Matlab on a HP Pavillion Laptop with Intel Core i7 2.60 GHz.

A detailed analysis showed that the bottleneck of Z and Ch-F is the evaluation of the angular exponential function. GH moments are the fastest because they are separable and do not contain any exponential terms. However, Appell moments are slower by one order only and faster than Z and Ch-F moments.

If we applied the moments repeatedly to many images/patches, we would pre-calculate the polynomials off-line and store their values. Then the moment computation would consist of element-wise matrix multiplication only, and its complexity would not depend on the polynomial basis.

7. Conclusion

We introduced new rotation moment invariants, which are composed of non-separable Appell moments. To our best knowledge, this is the first application of 2D non-separable polynomials in object recognition. The design of the invariants was possible thanks to our proof that the Appell polynomials are quasi-monomials. This is the major theoretical result of the paper. Furthermore, we proposed recursive formulae for their fast and stable computation.

To show the performance of the new Appell invariants in practice, we performed a huge number of recognition tests. The main conclusion is the following. The Appell invariants perform slightly better than Gaussian–Hermite invariants and significantly better than Zernike and Chebyshev–Fourier ones on both noise-free as well as noisy images. This is mainly due to more even distribution of zeros of the Appell polynomials over the image space, which leads to a better representation ability of the Appell moments, especially if only low-order features are used.

Declaration of Competing Interest

Authors declare that they have no conflict of interest.

Acknowledgments

This work has been supported by the Czech Science Foundation under the grant no. GA21-03921S and by the *Praemium Academiae*. L. Bedratyuk has been supported by the Ministry of Education and Science of Ukraine under the grant no. 0119U100662.

Appendix A. Proof of Theorem 1

We prove the forward implication first. We start with formulating an auxiliary lemma, that we later use to prove the statement of Theorem 1.

Lemma. Let $\{B_{m,n}(x,y)\}$ be a quasi-monomial family. Then the following identity holds

$$x\frac{\partial B_{m,n}(x,y)}{\partial y} - y\frac{\partial B_{m,n}(x,y)}{\partial x} = nB_{m+1,n-1}(x,y) - mB_{m-1,n+1}(x,y). \tag{A.1}$$

Proof. The identity follows immediately from differentiation of the relation

$$B_{m,n}(x',y') \equiv B_{m,n}(x\cos\theta - y\sin\theta, x\sin\theta + y\cos\theta) =$$
$$= \sum_{i=0}^{m}\sum_{j=0}^{n}(-1)^i\binom{m}{i}\binom{n}{j}(\cos\theta)^{n-i+j}(\sin\theta)^{n-j+i}B_{m+n-i-j,i+j}(x,y)$$

with respect to θ at $\theta = 0$. After a simplification, we obtain (A.1). □

We use the Lemma to investigate the derivatives of the generating function G

$$x\frac{\partial G}{\partial y} - y\frac{\partial G}{\partial x} = \sum_{m,n=0}^{\infty}\left(x\frac{\partial B_{m,n}(x,y)}{\partial y} - y\frac{\partial B_{m,n}(x,y)}{\partial x}\right)\frac{u^m}{m!}\frac{v^n}{n!} =$$
$$= \sum_{m,n=0}^{\infty}(nB_{m+1,n-1}(x,y) - mB_{m-1,n+1}(x,y))\frac{u^m}{m!}\frac{v^n}{n!} =$$
$$= v\sum_{m,n=0}^{\infty}B_{m+1,n-1}(x,y)\frac{u^m}{m!}\frac{v^{n-1}}{(n-1)!} -$$
$$u\sum_{m,n=0}^{\infty}B_{m-1,n+1}(x,y)\frac{u^{m-1}}{(m-1)!}\frac{v^n}{n!} = v\frac{\partial G}{\partial u} - u\frac{\partial G}{\partial v}.$$

Thus, G satisfies the partial differential equation

$$x\frac{\partial G}{\partial y} - y\frac{\partial G}{\partial x} = v\frac{\partial G}{\partial u} - u\frac{\partial G}{\partial v}. \tag{A.2}$$

Differential equation that contains a function of four variables cannot have more than three functionally independent solutions. However, $x^2+y^2, u^2+v^2,$ and $xu+yv$ are obviously its solutions and are independent. Hence, G must be a function of x^2+y^2, u^2+v^2, and $xu+yv$ only.

Now let us prove the reverse implication. Let

$$G(x,y,u,v) = G(xu+yv, x^2+y^2, u^2+v^2).$$

We have to prove that $\{B_{m,n}(x,y)\}$ is a quasi-monomial family.

Under the above assumption, G satisfies the identity $G(x', y', u, v) = G(x, y, \bar{u}, \bar{v})$, where (x', y') are rotated coordinates by θ (see Eq. (2)) and

$$\bar{u} = u\cos\theta + v\sin\theta,$$
$$\bar{v} = v\cos\theta - u\sin\theta.$$

To see that, it is sufficient to realize that $x'u + y'v = x\bar{u} + y\bar{v}$, $x'^2 + y'^2 = x^2 + y^2$ and $\bar{u}^2 + \bar{v}^2 = u^2 + v^2$.

Now we have, on the one hand,

$$G(x',y',u,v) = \sum_{m,n=0}^{\infty}B_{m,n}(x',y')\frac{u^m}{m!}\frac{v^n}{n!},$$

and on the other hand we get

$$G(x,y,\bar{u},\bar{v}) = \sum_{m,n=0}^{\infty}B_{m,n}(x,y)\frac{\bar{u}^m}{m!}\frac{\bar{v}^n}{n!}.$$

Comparing the right-hand sides and substituting for $\bar{u}$ and $\bar{v}$, we obtain

$$\sum_{m,n=0}^{\infty}B_{m,n}(x',y')\frac{u^m}{m!}\frac{v^n}{n!} = \sum_{m,n=0}^{\infty}B_{m,n}(x,y)\frac{(u\cos\theta + v\sin\theta)^m}{m!}\cdot$$
$$\cdot\frac{(v\cos\theta - u\sin\theta)^n}{n!}.$$

By equating the coefficients of the same powers of u and v we get

$$B_{m,n}(x',y') = \sum_{i=0}^{m}\sum_{j=0}^{n}(-1)^i\binom{m}{i}\binom{n}{j}(\cos\theta)^{m-i+j}(\sin\theta)^{n-j+i}\cdot$$
$$\cdot B_{m+n-i-j,i+j}(x,y),$$

which exactly matches Eq. (3). Therefore, $\{B_{m,n}(x,y)\}$ is a quasi-monomial family.

Appendix B. Proof of Theorem 2

If $\widetilde{B}_{m,n}(x,y) = \alpha_{m,n}B_{m,n}(x,y)$ is a quasi-monomial then it satisfies the identity (A.1)

$$x\frac{\partial\widetilde{B}_{m,n}}{\partial y} - y\frac{\partial\widetilde{B}_{m,n}}{\partial x} = n\widetilde{B}_{m+1,n-1} - m\widetilde{B}_{m-1,n+1}$$

which can be rewritten into the form

$$x\frac{\partial B_{m,n}}{\partial y} - y\frac{\partial B_{m,n}}{\partial x} = n\frac{\alpha_{m+1,n-1}}{\alpha_{m,n}}B_{m+1,n-1} - m\frac{\alpha_{m-1,n+1}}{\alpha_{m,n}}B_{m-1,n+1}$$

(we dropped the argument (x,y) for simplicity). We obtain a system of recurrent equations

$$\alpha_{m+1,n-1} = \alpha_{m,n},$$
$$\alpha_{m-1,n+1} = \alpha_{m,n}.$$

It is easily seen that a solution of the system is $\alpha_{m,n} = \phi(m+n)$ where ϕ is an arbitrary function.

Now let us prove the reverse implication. If $\alpha_{m,n} = \phi(m+n)$ for some ϕ, then obviously

$$\alpha_{m+1,n-1} = \alpha_{m,n},$$
$$\alpha_{m-1,n+1} = \alpha_{m,n}$$

and we get the following sequence of equalities

$$x\frac{\partial\widetilde{B}_{m,n}}{\partial y} - y\frac{\partial\widetilde{B}_{m,n}}{\partial x} = \alpha_{m,n}\left(x\frac{\partial B_{m,n}}{\partial y} - y\frac{\partial B_{m,n}}{\partial x}\right)$$
$$= \alpha_{m,n}(nB_{m+1,n-1} - mB_{m-1,n+1})$$
$$= n\widetilde{B}_{m+1,n-1} - m\widetilde{B}_{m-1,n+1}.$$

Hence, we have just proved that $\{\widetilde{B}_{m,n}\}$ satisfies the identity (A.1). The generating function

$$\widetilde{G}(x,y,u,v) = \sum_{m,n=0}^{\infty}\widetilde{B}_{m,n}(x,y)\frac{u^m}{m!}\frac{v^n}{n!}$$

fulfills the differential Eq. (A.2). According to Theorem 1, $\{\widetilde{B}_{m,n}\}$ must be a quasi-monomial family.

Appendix C. Proof of Theorem 3

The generating function

$$G(x,y,u,v)=\frac{1}{1-2(xu+yv)+u^2+v^2}$$

satisfies the following first-order differential equations

$$(x-u)\frac{\partial G}{\partial x}-u\frac{\partial G}{\partial u}=0\,,\qquad (y-v)\frac{\partial G}{\partial y}-v\frac{\partial G}{\partial v}=0\,,$$
$$(v-y)\frac{\partial G}{\partial x}+u\frac{\partial G}{\partial v}=0\,,\qquad v\frac{\partial G}{\partial x}-x\frac{\partial G}{\partial y}+v\frac{\partial G}{\partial u}=0.$$

Each of these differential equations implies certain differential recurrence relation for $V_{m,n}(x,y)$. For example, the first equation yields

$$\sum_{m,n=0}^{\infty}\left((x-u)\frac{\partial V_{m,n}(x,y)}{\partial x}\right)\frac{u^m}{m!}\frac{v^n}{n!}-\sum_{m,n=0}^{\infty}mV_{m,n}(x,y)\frac{u^m}{m!}\frac{v^n}{n!}=0\,,$$

and

$$\sum_{m,n=0}^{\infty}\left(x\frac{\partial V_{m,n}(x,y)}{\partial x}-\frac{\partial V_{m-1,n}(x,y)}{\partial x}-mV_{m,n}(x,y)\right)\frac{u^m}{m!}\frac{v^n}{n!}=0\,,$$

which leads to the identity

$$x\frac{\partial V_{m,n}(x,y)}{\partial x}=mV_{m,n}(x,y)+m\frac{\partial V_{m-1,n}(x,y)}{\partial x}. \tag{C.1}$$

In a similar way, we find the following three differential recurrence equations

$$y\frac{\partial V_{m,n}(x,y)}{\partial x}=n\frac{\partial V_{m,n-1}(x,y)}{\partial x}+mV_{m-1,n+1}(x,y)\,, \tag{C.2}$$

$$x\frac{\partial V_{m,n}(x,y)}{\partial y}=m\frac{\partial V_{m-1,n}(x,y)}{\partial y}+nV_{m+1,n-1}(x,y), \tag{C.3}$$

$$y\frac{\partial V_{m,n}(x,y)}{\partial y}=nV_{m,n}(x,y)+n\frac{\partial V_{m,n-1}(x,y)}{\partial y}. \tag{C.4}$$

Let us derive two more auxiliary recurrences. We have

$$1=\left[1-2(xu+yv)+u^2+v^2\right]\sum_{m,n=0}^{\infty}V_{m,n}(x,y)\frac{u^m}{m!}\frac{v^n}{n!}=$$
$$=\sum_{m,n=0}^{\infty}\left[1-2(xu+yv)+u^2+v^2\right]V_{m,n}(x,y)\frac{u^m}{m!}\frac{v^n}{n!}.$$

With the same considerations as for (C.1) and after the index shifting $m\mapsto m+1$ we get

$$2(1+m)xV_{m,n}(x,y)+2nyV_{m+1,n-1}(x,y)=V_{m+1,n}(x,y)$$
$$+m(m+1)V_{m-1,n}(x,y)+n(n-1)V_{m+1,n-2}(x,y). \tag{C.5}$$

We derive another auxiliary recurrence

$$xV_{m,n}(x,y)-yV_{m+1,n-1}(x,y)=mV_{m-1,n}(x,y)-(n-1)V_{m+1,n-2}(x,y). \tag{C.6}$$

When shifting the indices $m\mapsto m+1$ and $n\mapsto n-1$ in (C.2) and subtracting the result from (C.1), we obtain

$$V_{m,n}(x,y)+x\frac{\partial V_{m,n}(x,y)}{\partial x}-y\frac{\partial V_{m+1,n-1}(x,y)}{\partial x}$$
$$=m\frac{\partial V_{m-1,n}(x,y)}{\partial x}-(n-1)\frac{\partial V_{m+1,n-2}(x,y)}{\partial x}.$$

This equation can be equivalently rewritten into the form

$$\frac{\partial}{\partial x}(xV_{m,n}(x,y)-yV_{m+1,n-1}(x,y))$$
$$=\frac{\partial}{\partial x}(mV_{m-1,n}(x,y)-(n-1)V_{m+1,n-2}(x,y)).$$

By integrating this we get

$$xV_{m,n}(x,y)-yV_{m+1,n-1}(x,y)=mV_{m-1,n}(x,y)$$
$$-(n-1)V_{m+1,n-2}(x,y)+C_{m,n}(y), \tag{C.7}$$

where $C_{m,n}(y)$ is a function of single variable y. Similarly, differentiating (C.7) with respect to y and taking (C.3) and (C.4) into account, we get that $C'_{m,n}(y)=0$. Thus, $C_{m,n}(y)$ is a constant $C_{m,n}$. Substituting $x=y=0$ into (C.7) we obtain that $C_{m,n}=0$.

Multiplying now (C.6) by $2n$ and then adding it to (C.5) we obtain

$$2(1+m+n)xV_{m,n}(x,y)=V_{m+1,n}(x,y)-n(n-1)V_{m+1,n-2}(x,y)$$
$$+m(m+2n+1)V_{m-1,n}(x,y),$$

as required.

In the same way we prove the second recurrence relation (8).

Appendix D. Proof of Theorem 4

By a direct calculation one may show that the generating function

$$G(x,y,u,v)=\frac{1}{[(1-(ux+vy))^2-(u^2+v^2)(x^2+y^2-1)]^{\frac{1}{2}}}$$

satisfies the following two first-order differential equations

$$x\left(2u\frac{\partial G}{\partial u}+v\frac{\partial G}{\partial v}+G\right)+yu\frac{\partial G}{\partial v}=\frac{\partial(u^2G)}{\partial u}+v\frac{\partial uG}{\partial v}-uG+\frac{\partial G}{\partial u}\,,$$
$$y\left(2v\frac{\partial G}{\partial v}+u\frac{\partial G}{\partial u}+G\right)+xv\frac{\partial G}{\partial u}=\frac{\partial(v^2G)}{\partial v}+vu\frac{\partial G}{\partial u}-vG+\frac{\partial G}{\partial v}.$$

These equations imply the recurrences

$$(n+2m+1)xU_{m,n}(x,y)+myU_{m-1,n+1}(x,y)$$
$$=m(m+n)U_{m-1,n}(x,y)+U_{m+1,n}(x,y),$$

$$(m+2n+1)yU_{m,n}(x,y)+nxU_{m+1,n-1}(x,y)$$
$$=n(m+n)U_{m,n-1}(x,y)+U_{m,n+1}(x,y). \tag{D.2}$$

When shifting the index $m\mapsto m-1$ in (D.2)

$$(m+2n)yU_{m-1,n}(x,y)+nxU_{m,n-1}(x,y)$$
$$=n(m+n-1)U_{m-1,n-1}(x,y)+U_{m-1,n+1}(x,y),$$

we eliminate $U_{m-1,n+1}(x,y)$ from (D.1) and obtain

$$U_{m+1,n}(x,y)=(n+2m+1)xU_{m,n}+mnxyU_{m,n-1}$$
$$-mn(m+n-1)yU_{m-1,n-1}$$
$$+m\left[(y^2-1)m+n(2y^2-1)\right]U_{m-1,n}$$

as required. In a similar way, we prove that

$$U_{m,n+1}(x,y)=(m+2n+1)yU_{m,n}+mnxyU_{m-1,n}$$
$$-mn(m+n-1)xU_{m-1,n-1}$$
$$+n\left[(x^2-1)n+m(2x^2-1)\right]U_{m,n-1}.$$

Appendix E. Recurrent relations for the normalized AP's

Recurrence for the V-family

$$\widetilde{V}_{m,m}=\sqrt{\frac{\Gamma(m+0.5)}{\Gamma(m+1)}}\frac{2m+1}{(2m)^{3/4}}\left[x\widetilde{V}_{m-1,m}+y\widetilde{V}_{m,m-1}\right]$$
$$-\frac{(m-1)(2m+1)}{(8m)^{1/4}(2m-1)^{7/4}}\left[\widetilde{V}_{m-2,m}+\widetilde{V}_{m,m-2}\right],$$

$$\widetilde{V}_{m,n+1}=2\frac{m+n+2}{(m+n+1)^{7/4}}\sqrt{\frac{\Gamma\left(\frac{m+n+2}{2}\right)}{\Gamma\left(\frac{m+n+3}{2}\right)}}\left[mx\widetilde{V}_{m-1,n+1}+(n+1)y\widetilde{V}_{m,n}\right]-$$

$$-\frac{\sqrt{2}(m+n+2)}{(m+n)^{7/4}(m+n+1)^{5/4}}\left[n(n+1)\widetilde{V}_{m,n-1}+m(m-1)\widetilde{V}_{m-2,n+1}\right].$$

Recurrence for the U-family

$$\begin{aligned}
\widetilde{U}_{m,m} =& x\left[\sqrt{\frac{\Gamma(m+0.5)}{\Gamma(m+1)}}\frac{3m-1}{(2m)^{3/4}}\widetilde{U}_{m-1,m}\right.\\
&\left.+\frac{m-1}{(8m)^{1/4}(2m-1)^{3/4}}y\widetilde{U}_{m-1,m-1}\right]+\\
&+(m-1)\left\{\frac{y^2(3m-1)-2m+1}{m^{5/4}(4m-2)^{3/4}}\widetilde{U}_{m-2,m}\right.\\
&\left.-\sqrt{\frac{\Gamma(m-0.5)}{\Gamma(m+1)}}\frac{[2m(m-1)]^{1/4}}{(4m-2)^{3/4}}y\widetilde{U}_{m-2,m-1}\right\},\\
\widetilde{U}_{m,n+1} =& \sqrt{\frac{\Gamma\left(\frac{m+n+2}{2}\right)}{\Gamma\left(\frac{m+n+3}{2}\right)}}\frac{m+2n+1}{(m+n+1)^{3/4}}y\widetilde{U}_{m,n}\\
&-\sqrt{\frac{\Gamma\left(\frac{m+n}{2}\right)}{\Gamma\left(\frac{m+n+3}{2}\right)}}\frac{mn(m+n+1)^{1/4}}{[(m+n+1)(m+n)]^{3/4}}x\widetilde{U}_{m-1,n-1}+\\
&+\frac{\sqrt{2}n}{(m+n+1)^{5/4}(m+n)^{3/4}}\left\{mxy\widetilde{U}_{m-1,n}+\left[\left(x^2-1\right)n\right.\right.\\
&\left.\left.+m\left(2x^2-1\right)\right]\widetilde{U}_{m,n-1}\right\},\\
\widetilde{U}_{n+1,m} =& \sqrt{\frac{\Gamma\left(\frac{m+n+2}{2}\right)}{\Gamma\left(\frac{m+n+3}{2}\right)}}\frac{m+2n+1}{(m+n+1)^{3/4}}x\widetilde{U}_{n,m}\\
&-\sqrt{\frac{\Gamma\left(\frac{m+n}{2}\right)}{\Gamma\left(\frac{m+n+3}{2}\right)}}\frac{mn(m+n+1)^{1/4}}{[(m+n+1)(m+n)]^{3/4}}y\widetilde{U}_{n-1,m-1}+\\
&+\frac{\sqrt{2}n}{(m+n+1)^{5/4}(m+n)^{3/4}}\left\{mxy\widetilde{U}_{n,m-1}\right.\\
&\left.+\left[\left(y^2-1\right)n+m\left(2y^2-1\right)\right]\widetilde{U}_{n-1,m}\right\}.
\end{aligned}$$

We dropped the argument (x, y) for simplicity.

References

[1] J. Flusser, T. Suk, B. Zitová, 2D and 3D Image Analysis by Moments, Wiley, Chichester, U.K., 2016.
[2] Y.S. Abu-Mostafa, D. Psaltis, Recognitive aspects of moment invariants, IEEE Trans. Pattern Anal. Mach. Intell. 6 (6) (1984) 698–706.
[3] M.-K. Hu, Visual pattern recognition by moment invariants, IRE Trans. Inf. Theory 8 (2) (1962) 179–187.
[4] C.-H. Teh, R.T. Chin, On image analysis by the method of moments, IEEE Trans. Pattern Anal. Mach. Intell. 10 (4) (1988) 496–513.
[5] M. Pawlak, Image Analysis by Moments: Reconstruction and Computational Aspects, Oficyna Wydawnicza Politechniki Wrocławskiej, Wrocław, Poland, 2006.
[6] K.M. Hosny, New set of rotationally Legendre moment invariants, Int. J. Electr., Comput., Syst. Eng. 4 (3) (2010) 176–180.
[7] R. Mukundan, S.H. Ong, P.A. Lee, Image analysis by Tchebichef moments, IEEE Trans. Image Process. 10 (9) (2001) 1357–1364.
[8] R. Mukundan, Some computational aspects of discrete orthonormal moments, IEEE Trans. Image Process. 13 (8) (2004) 1055–1059.
[9] J. Flusser, J. Kautsky, F. Šroubek, Implicit moment invariants, Int. J. Comput. Vis. 86 (1) (2010) 72–86.
[10] J. Shen, Orthogonal Gaussian–Hermite moments for image characterization, in: D.P. Casasent (Ed.), Intelligent Robots and Computer Vision XVI: Algorithms, Techniques, Active Vision, and Materials Handling, vol. 3208, SPIE, 1997, pp. 224–233.
[11] J. Shen, W. Shen, D. Shen, On geometric and orthogonal moments, Int. J. Pattern Recognit. Artif Intell. 14 (7) (2000) 875–894.
[12] B. Yang, G. Li, H. Zhang, M. Dai, Rotation and translation invariants of Gaussian–Hermite moments, Pattern Recognit. Lett. 32 (2) (2011) 1283–1298.
[13] B. Yang, M. Dai, Image analysis by Gaussian–Hermite moments, Signal Process. 91 (10) (2011) 2290–2303.
[14] P.-T. Yap, R. Paramesran, S.-H. Ong, Image analysis by Krawtchouk moments, IEEE Trans. Image Process. 12 (11) (2003) 1367–1377.
[15] S.X. Liao, A. Chiang, Q. Lu, M. Pawlak, Chinese character recognition via Gegenbauer moments, in: Proceedings of the 16th International Conference on Pattern Recognition ICPR'02, vol. 3, IEEE Computer Society, 2002, pp. 485–488.
[16] M.R. Teague, Image analysis via the general theory of moments, J. Opt. Soc. Am. 70 (8) (1980) 920–930.
[17] A. Khotanzad, Y.H. Hong, Invariant image recognition by Zernike moments, IEEE Trans. Pattern Anal. Mach. Intell. 12 (5) (1990) 489–497.
[18] Å. Wallin, O. Kübler, Complete sets of complex Zernike moment invariants and the role of the pseudoinvariants, IEEE Trans. Pattern Anal. Mach. Intell. 17 (11) (1995) 1106–1110.
[19] S.O. Belkasim, M. Shridhar, M. Ahmadi, Pattern recognition with moment invariants: A comparative study and new results, Pattern Recognit. 24 (12) (1991) 1117–1138.
[20] Y. Sheng, J. Duvernoy, Circular-Fourier-radial-Mellin transform descriptors for pattern recognition, J. Opt. Soc. Am. A 3 (6) (1986) 885–888.
[21] Y. Sheng, L. Shen, Orthogonal Fourier–Mellin moments for invariant pattern recognition, J. Opt. Soc. Am. A 11 (6) (1994) 1748–1757.
[22] Z. Ping, H. Ren, J. Zou, Y. Sheng, W. Bo, Generic orthogonal moments: Jacobi–Fourier moments for invariant image description, Pattern Recognit. 40 (4) (2007) 1245–1254.
[23] Z. Ping, R. Wu, Y. Sheng, Image description with Chebyshev–Fourier moments, J. Opt. Soc. Am. A 19 (9) (2002) 1748–1754.
[24] K.M. Hosny, M.M. Darwish, New set of multi-channel orthogonal moments for color image representation and recognition, Pattern Recognit. 88 (2019) 153–173.
[25] C. Di Ruberto, L. Putzu, G. Rodriguez, Fast and accurate computation of orthogonal moments for texture analysis, Pattern Recognit. 83 (2018) 498–510.
[26] M. Nwali, S. Liao, A new fast algorithm to compute continuous moments defined in a rectangular region, Pattern Recognit. 89 (2019) 151–160.
[27] H.-Y. Yang, S.-R. Qi, C. Wang, S.-B. Yang, X.-Y. Wang, Image analysis by log-polar exponent-Fourier moments, Pattern Recognit. 101 (2020) 107177.
[28] R. Benouini, I. Batioua, K. Zenkouar, A. Zahi, S. Najah, H. Qjidaa, Fractional-order orthogonal Chebyshev moments and moment invariants for image representation and pattern recognition, Pattern Recognit. 86 (2019) 332–343.
[29] K.M. Hosny, M.M. Darwish, T. Aboelenen, New fractional-order Legendre–Fourier moments for pattern recognition applications, Pattern Recognit. 103 (2020) 107324.
[30] H. Yang, S. Qi, J. Tian, P. Niu, X. Wang, Robust and discriminative image representation: fractional-order Jacobi–Fourier moments, Pattern Recognit. 115 (2021) 107898.
[31] J. Flusser, On the independence of rotation moment invariants, Pattern Recognit. 33 (9) (2000) 1405–1410.
[32] L. Bedratyuk, 2D geometric moment invariants from the point of view of the classical invariant theory, J. Math. Imaging Vis. 62 (2020) 1062–1075.
[33] B. Yang, J. Flusser, T. Suk, Design of high-order rotation invariants from Gaussian–Hermite moments, Signal Process. 113 (1) (2015) 61–67.
[34] B. Yang, J. Flusser, J. Kautsky, Rotation of 2D orthogonal polynomials, Pattern Recognit. Lett. 102 (1) (2018) 44–49.
[35] F. Didon, Étude de certaines fonctions analogues aux fonctions X_n de Legendre, etc, in: Annales Scientifiques de l'École Normale Supérieure, vol. 5, 1868, pp. 229–310.
[36] J. Favard, Sur les polynômes de Tchebicheff, C. R. Acad. Sci. Paris 200 (2052–2055) (1935) 11.
[37] Y. Jiang, Z. Ping, L. Gao, A fast algorithm for computing Chebyshev–Fourier moments, in: International Seminar on Future Information Technology and Management Engineering FITME'10, IEEE, 2010, pp. 425–428.
[38] E.C. Kintner, On the mathematical properties of Zernike polynomials, J. Mod. Opt. 23 (8) (1976) 679–680.
[39] B. Li, G. Zhang, B. Fu, Image analysis using radial Fourier-Chebyshev moments, in: International Conference on Multimedia Technology ICMT'11, IEEE, 2011, pp. 3097–3100.
[40] Amsterdam library of object images (ALOI), 2005, https://aloi.science.uva.nl/.

Leonid Bedratyuk received the Ph.D. degree in mathematics from the Moscow State University in 1995 and the Dr.Sc. degree in mathematics from the National Academy of Sciences of Ukraine in 2012. Currently he is a professor of the Khmelnytsky National University, Ukraine. His research interests centre on invariant theory and its applications.

Jan Flusser received the M.Sc. degree in mathematical engineering from the Czech Technical University, Prague, Czech Republic, in 1985; the Ph.D degree in computer science from the Czechoslovak Academy of Sciences in 1990; and the Dr.Sc. degree in technical cybernetics in 2001. Since 1985 he has been with the Institute of Information Theory and Automation, Czech Academy of Sciences, Prague. In 1995–2007, he was holding the position of a head of Department of Image Processing. In 2007–2017, he was a Director of the Institute. Since 2017 he has been at the position of Research Director. He is a full professor of computer science at the Czech Technical University, Faculty of Nuclear Science and Physical Engineering, and at the Charles University, Faculty of Mathematics and Physics, Prague, Czech Republic, where he gives undergraduate and graduate courses on Digital Image Processing, Pattern Recognition, and Moment Invariants and Wavelets. Jan Flusser's research interest covers moments and moment invariants, image registration, image fusion, multichannel blind deconvolution, and super-resolution imaging. He has authored and coauthored more than 200 research publications in these areas, including the monographs Moments and Moment Invariants in Pattern Recognition (Wiley, 2009)

and 2D and 3D Image Analysis by Moments (Wiley, 2016). In 2010, Jan Flusser was awarded by the SCOPUS 1000 Award. He received the Felber Medal of the Czech Technical University for excellent contribution to research and education in 2015 and the Praemium Academicae of the Czech Academy of Sciences for outstanding researchers in 2017.

Tomáš Suk received the M.Sc. degree in electrical engineering from the Czech Technical University, Faculty of Electrical Engineering, Prague, Czech Republic, in 1987, the Ph.D degree in computer science from the Czechoslovak Academy of Sciences in 1992, and the D.Sc. degree from the Czech Academy of Sciences in 2018. Since 1991 he has been a researcher with the Institute of Information Theory and Automation, Czech Academy of Sciences, Prague. He has authored more than 35 journal papers, more than 50 conference papers and coauthored the monographs Moments and Moment Invariants in Pattern Recognition (Wiley, 2009) and 2D and 3D Image Analysis by Moments (Wiley, 2016). Tomas Suk's research interests include digital image processing, pattern recognition, image filtering, invariant features, moment-based and point-based invariants, spatial transformations of images, and applications in remote sensing, astronomy, botany, medicine, and computer vision. In 2002, Tomas Suk received the Otto Wichterle Premium of the Czech Academy of Sciences for excellent young scientists.

Jitka Kostková received the M.Sc. degree in Applied Mathematical Stochastic Methods from the Czech Technical University, Faculty of Nuclear Science and Physical Engineering, Prague, Czech Republic, in 2015 and the Ph.D. degree in Mathematical Engineering from the same university in 2020, under the supervision of Jan Flusser. Currently she is a postdoc in the Institute of Information Theory and Automation, Prague, Czech Republic, and a tutor of undergraduate courses on calculus. Her research interest is focused on moments and moment invariants. Jitka Kostkova was awarded by the Joseph Fourier Prize in 2020 and by the Antonin Svoboda Award in 2021.

Jaroslav Kautsky received the M.Sc. degree in mathematics from the Charles University, Prague, Czech Republic, in 1957 and the Ph.D. degree in mathematicsin 1961 from the Czechoslovak Academy of Sciences, Prague, where he held research positions in the Institute of Mathematics until 1968. Since 1966, he has taught mathematics in Australia, first at the University of Adelaide, Adelaide, SA, Australia, from 1966 to 1969 and then at the Flinders University of South Australia, Adelaide, SA, where he has been an Honorary Research Fellow since retiring in 1987. For over 15 years, he has been a Regular Visiting Scientist in the Institute of Information Theory and Automation, Academy of Sciences of the Czech Republic, Prague, where he participated in research on invariants and wavelets. He was also a Principal Scientist at Prometheus Inc., Newport, RI. He has published about 60 papers in numerical analysis, particularly on integration, orthogonal polynomials, in control theory, numerical linear algebra, wavelets, and signal and image processing. In 2013, Jaroslav Kautsky was awarded by the Honourable Medal of Bernard Bolzano, presented by the Czech Academy of Sciences. Regretfully, Jaroslav Kautsky passed away in February 2021.